Proc. of SPIE 2013 Vol. 8957, 895701-895709

# 3D metallic nanostructures for bulk and bio-SPR sensing applications

Mohamadreza Najiminaini[a,b,c], Erden Ertorer[d,e], Hao Jiang[b], Bozena Kaminska[b], Silvia Mittler[d] and Jeffrey J.L. Carson[a,c,*]

[a]Imaging Program, Lawson Health Research Institute, St. Joseph's Health Care, London, ON, Canada

[b]The School of Engineering Science, Simon Fraser University, Burnaby, BC, Canada

[c]The Department of Medical Biophysics, Schulich School of Medicine and Dentistry, University of Western Ontario, London, ON, Canada

[d]The Department of Physics and Astronomy, University of Western Ontario, London, ON, Canada

[e]Biomedical Engineering Program, Faculty of Engineering, University of Western Ontario, London, ON, Canada

## ABSTRACT

We present a 3D metallic nanostructure, which has transmission resonance properties related to both localized surface plasmons (LSP) and propagating surface plasmon polaritons (SPP). Various geometrical dimensions of the 3D metallic nanostructures were studied by means of simulation and experiment with respect to resonance position, resonance line width and bulk sensitivity. Narrower resonance line width and higher bulk sensitivity were achieved for the 3D nanostructure compared to conventional nanohole arrays. Finally, a 3D metallic nanostructure functionalized with a biotinylated thiol could detect streptavidin, suggesting the device may have potential as a bio- sensor.

**Keywords:** localized surface plasmon resonace (LSPR), surface plasmon resonance (SPR), sensing, extraordinary optical transmission (EOT), nano-hole array, 3D nanostructure, electron beam lithography (EBL).

## 1. INTRODUCTION

Surface plasmon resonance (SPR) sensing is one of the most common applications of metallic nanostructures and has been used widely for chemical detection, including bio-molecule sensing [1-3]. The SPR sensing principle is based on the change in optical resonance position due to a change in refractive index at the nanostructure surface [4]. An array of periodic holes in a metal film is a well-studied metallic nanostructure for SPR sensing applications [5,6]. The transmission-based SPRs of a nano-hole array (NHA) result from the interaction of light with the surface plasmon (i.e. a collective oscillation of the free electron gas at the interface between a metal and a dielectric). The SPR-light interaction provides an optical mechanism for detection of chemicals and bio-molecules that exploits the SPR properties of the NHA[SM1] [6]. The bulk sensitivity and the figure of merit (FOM) are two important metrics for evaluating the NHA sensor performance [7-9]. The bulk sensitivity is calculated from the SPR shift per refractive index unit (RIU) and the FOM is computed from the ratio of the bulk sensitivity and the line width (FWHM) of the SPR peak [4]. Many studies have investigated methods, such as alterations of the NHA feature shape and arrangement, in an attempt to improve the bulk sensitivity and FOM of metallic NHAs [4,7,10]. It has been shown that a NHA with ultra-smooth metallic surfaces and fewer imperfections in the nano-holes has improved bulk sensitivity and FOM [11]. Also, a NHA consisting of a double-hole with sharp apexes demonstrated an increased bulk sensitivity due to the higher localized electric field at the apexes of the double-hole at the SPR resonance [12]. Moreover, an index-matched condition between the NHA substrate and analyte on top surface of the NHA leading to a symmetric structure has proven improving the sensing performance [9,13].

A NHA with low hole-count (fewer than 100) has a poorer SPR sensing performance compared to a NHA with high hole count [8]. The higher performance of the NHA with high hole count is due to a narrower SPR peak width and the therefore increased slope of the SPR curve [14]. The bulk sensitivity and FOM for a NHA with low hole count were reported as

*jcarson@lawsonimaging.ca; phone 1 (519) 646-6100 x64767; www.lawsonimaging.ca/imaging/scientists

286 nm/RIU and 4.1 1/RIU, respectively [8]. SAttempts to improve SPR sensing performance of NHAs have been attempted by incorporating Bragg reflectors around the NHA structure [15,16]. Our group has recently reported that a low hole count NHA benefiting from dynamic SP energy matching between the top and bottom of the NHA had a 1.6-fold improvement in SPR sensitivity compared to a conventional NHA structure [9]. [SM2]The NHA with the SPR-matched property had a cavity integrated into the substrate, which allowed the analyte to flow to the underside of the NHA structure. Furthermore, we introduced a 3D metallic nanostructure consisting of co-registered nanoholes and nanodisks with a nano-sized separation distance [17]. This 3D nanostructure exhibited transmission resonances due to coupled LSPR interactions between nanoholes and nanodisks through enhanced electric fields. Although the 3D metallic nanostructure had a higher bulk sensitivity than the low hole count NHA withouta cavity, the resonance peak width was broader.[SM3]

Building upon these prior results, the objective here was to design a compact 3D metallic nanostructure with higher bulk sensitivity and FOM than previous low hole count NHA structures. This goal could be achieved by designing a 3D nanostructure, that benefits from dynamic SP energy matching, having enhanced electric fields around the structure, and utilizing an ultra-flat metal surface. Therefore, we designed and fabricated a 3D nanostructure consisting of a gold film containing a NHA with an underlying cavity and a gold nanocone array (NCA) at the bottom of the cavity. The combined NHA and NCA structures generate transmission resonances due to the LSPR and SPP interactions. The transmission resonances of the 3D nanostructures were studied experimentally and by simulations. Sensing performance of the 3D nanostructure was tested for bulk refractive index changes and for sensing of streptavidin, a protein binding to biotin (vitamin H).

## 2. METHODS

### 2.1 Fabrication

We employed electron beam lithography (EBL), a lift-off process, etching, [SM4]and deposition of gold with the goal of fabricating 3D nanostructures containing co-registered nanoholes and nanocones at the bottom of a cavity. First, a 3-nm thick titanium (Ti, source, grade) conductive layer was evaporated (what machine, type, company, from where, on to a Pyrex substrate (from what company?) yielding a conductive substrate for the EBL process. A negative photo-resist (ma-N 2403, MicroChem Corp., Newton Upper Falls, MA, USA) was spin-coated with 1000 RPM and soft-baked at 90 °C for 60 s in an oven on a hot plate????. [SM5]As a result, a 500-nm thick layer of photo-resist was formed on top of the 3-nm Ti sacrificial layer. A square NHA pattern (with an area of 25 $\mu m^2$) was written using an EBL in an electron microscope (LEO 1530, e-beam lithography, Zeiss, Oberkochen, Germany). The sample was developed for 40 s in MF-319 developer (Shipley Company, Marlborough, MA, USA) leaving behind photo-resist pillars. Then the sample was left under oxygen plasma (company, type, how many Watt power) for 30 s to remove photo-resist residue between adjacent pillars. Another 3-nm-thick Ti adhesion layer was deposited followed by evaporation (machine company, where?)of an 80-nm-thick gold layer (source, grade) onto the sample. In the lift-off process, the sample was left in remover PG (MicroChem Corp., city, country) at 80ºC (in an oven on a hot plate??) to remove pillars and leave behind a NHA in a gold film. In order to create a large 250-nm-deep cavity in the Pyrex substrate, the sample was left for 70 s in Ti etchant TFT, Transene company, Inc., Danvers, MA, USA). The Ti etchant (was used to isotropically wetchemically-etch the Pyrex substrate as well as the Ti adhesion and conductive layers. Finally, a 150-nm-thick layer of gold was evaporated on top of the NHA structure resulting in the 3D nanostructure (NHA-NCA) with 150-nm-tall nanocones at the bottom of the cavity below the NHA in the230-nm-thick gold film. We fabricated a series of 3D nanostructures of various periodicities (400 nm, 475 nm, and 550 nm), but fixed cavity depth of 250 nm fixed230-nm-thick gold film, and fixed 150-nm-thick nanocone at the bottom of the cavity. The ratio of nanohole area to background area (square of periodicity) was 0.09 for all 3D nanostructures. Figure 1 shows an SEM image of a NHA-NCA structure with 500-nm periodicity.. Each nanocone was circular [SM6]and had a truncated apex. The base diameter of each nanocone was approximately equal to the nanohole diameter measured before the 150-nm-thick gold deposition. The diameter of the truncated apex of each nanocone was close to a half of the diameter of the base. The truncated apex diameter of each nanocone was dependent on the deposition rate of the gold. For the fabricated 3D nanostructures, the gold deposition rate was set to 0.1 nm/s. The diameter of each nanohole at the top and the bottom surfaces of the gold film was approximately equal to the base of each gold nanocone. Also, the nanohole diameter decreased from both the top and the bottom surfaces to the middle of the gold film.

### 2.2 Finite Difference Time Domain (FDTD) simulation

We used the three-dimensional (3D) FDTD method to simulate the interaction between incident light and the 3D gold nanostructures for assessing the optical transmission properties. The FDTD solution package from Lumerical Inc. (Vancouver, Canada) was employed to simulate the optical characteristics of the truncated nanocone array (NCA) and the NHA-NCA. In the simulation model, a plain wave source was used and was incident normal to the plane of the nanocone base from the top. The dielectric function of the gold was taken from Palik [18]. The dielectric constants of the substrate and surrounding media were set to the dielectric constant of Pyrex (n=1.474 at λ=587 nm) [source of numbers] and the dielectric constant of water (n=1.33 at λ=587 nm) [source]. The boundary conditions were set to periodic and perfectly matched layers (PML) for the *xy* and the *z* boundaries, respectively.

Nanocone arrays with various base and apex diameters (apex diameter was half of the base diameter) were simulated. The nanocone base diameters varied between 140 nm and 192 nm in 8-nm increments. Also, the refractive index of the surrounding medium was varied between 1.30 and 1.39 in 0.03 increments to assess the bulk sensitivity of each resonance. The NHA-NCAs with 400-nm, 475-nm and 550-nm periodicities were simulated to compare with experimental results. The NHA-NCA geometrical dimensions for each 3D structure were set to measured values from the fabricated structures.

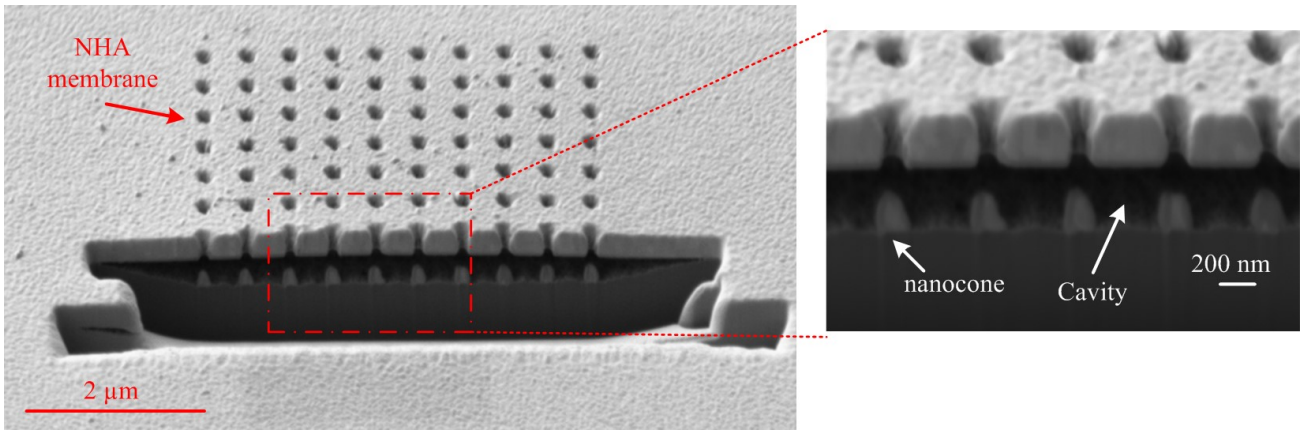


Figure 1. SEM image of a 3D nanostructure with 500-nm periodicity (230-nm-thick gold NHA film and a 150-nm-tall NCA at bottom of the cavity). The top and bottom surface diameters of the holes and the base diameter of the cones were 175 nm. The apex diameter of the cone and the hole diameter at the mid-depth of each hole were approximately 90 nm.

### 2.3 Optical transmission setup

We used a standard inverted microscope (Nikon, TE300, Tokyo, Japan) attached to a photometer (PTI, D104, from where), monochromator (PTI, 101, where? London, Ontario, Canada?), and photo-multiplier (PTI, 710 where) for measuring transmission spectra of each 3D nanostructure. Unpolarized white light from a 100 W halogen lamp ( company, where) was focused on the sample using the bright-field condenser lens (NA = 0.3) of the microscope (Nikon, 40 x or 100 x or ???. The transmitted light was collected with a 20× objective (NA = 0.45; Nikon, 93150) and reflected by a beam splitter to the photometer. A desired region of a given sample was chosen using the aperture adjustment on the photometer. Light from the selected region reached the monochromator for spectral characterization and detection by the photo-multiplier tube. The optical transmission spectra were computed by subtracting the background signals [SM7](dark noise) from the spectra transmitted through the NHA-NCA and then dividing the result [SM8]by the measured white light spectrum from halogen lamp.

### 2.4 Bulk sensing

A transmission spectrum of each 3D nanostructure was measured for each liquid refractive index standard (Cargille Laboratories, Cedar Grove, NJ, USA) between 1.30 and 1.39 in increments of 0.03. The liquids were applied to the top surface of the 3D nanostructures. Due to capillary forces, liquid penetrated into the cavity of each 3D nanostructure. The bulk sensitivity was assessed from the slope of the line depicting the  fit of the resonance position versus refractive index.

### 2.5 Bio-sensing of streptavidin

To prepare the sensor for detection of streptavidin, each 3D nanostructure was first placed in a UV-ozone oven (type, company, power in Watt) for 30 minutes cleaning the gold surfaces. Then, the gold surfaces of each 3D nanostructure were functionalized with a binary mixture of an OH-terminated and biotinylated thiol for 24 hours. This process generated biotin recognition sites in a self-assembled monolayer for binding streptavidin without steric hindrance [Spinke et al.]. The solution for the functionalization process contained anhydrous ethanol, 0.45-mM 11-mercaptoundecanol (Sigma-Aldrich, Ontario, Canada), and 0.05-mM biotinylated thiol (NanoScience Chemicals, Phoenix, AZ, USA). The device was then rinsed with ethanol and dried with nitrogen. Finally, the sample was immersed in PBS buffer and streptavidin (Rockland Inc., PA, USA) was mixed into the PBS buffer at different concentrations.

## 3. RESULTS AND DISCUSSION

Figure 2 (a) displays simulated optical transmission data of NCAs with various base and apex diameters (apex diameter was half of the base diameter for all NCAs) and a 150-nm-thick gold nanocone. Two LSPRs were observed in the transmission spectra of each NCA. The LSPR absorption at longer and shorter wavelengths were due to the excitation of LSPs at the base and the apex of the nanocones, respectively. It was observed that as the base diameter of the nanocone increased the LSPR position red-shifted for both LSPRs related to the apex and base. Electric field distributions of a nanocone at the LSPRs of the NCA structures (shown in Figure 2 (a)) are illustrated in Figure 2 (b). Figure 2 (b) clearly demonstrates that the LSPRs were associated with excitation of the LSPRs at the apex or base . The electric field distributions of the LSPRs around both the apex and base of a nanocone have a dipolar mode since two intensified electric fields (hot spots) exist at opposite ends of the nanocone. The electric field distribution was larger for the nanocone with the larger base and apex diameters.[SM9] This was expected since the SPR decay length into the dielectric or metal materials increases as a function of wavelength [19]. Figure 2 (c) displays the LSPR spectral absorption positions related to the LSPR excitation related to the apex and base of the nanocone as a function of base diameter. The spectral LSPR absorption position from the base side of a nanocone showed a larger red-shift compared to that of the apex side of the nanocone. The LSPR shifts were found to be linearly dependent on the base diameter. Furthermore, the LSPRs of a NCA with 166-nm-base and 88-nm-apex diameters were shown for various refractive indexes between 1.30 and 1.39 in Figure 2 (d). The bulk sensitivities of LSPRs related to the apex and base cases were 443 nm/RIU and 233 nm/RIU, respectively. Since the apex side of the nanocone was fully contained in refractive index of the medium, it had a higher bulk sensitivity compared to that of the base side. The lower bulk sensing of the LSPR related to the base side was expected, because the bottom side of the base was in contact with the Pyrex substrate and its overall bulk sensitivity was affected by the unchanging Pyrex refractive index. Although the bulk sensitivity of the LSPR related to the apex of the nanocone had a larger sensitivity, the width of the LSPR peak was similar, but had lower absorption compared to the base. As a result, this was expected to significantly degrade the FOM of the LSPRs related to the apex side of the nanocone.

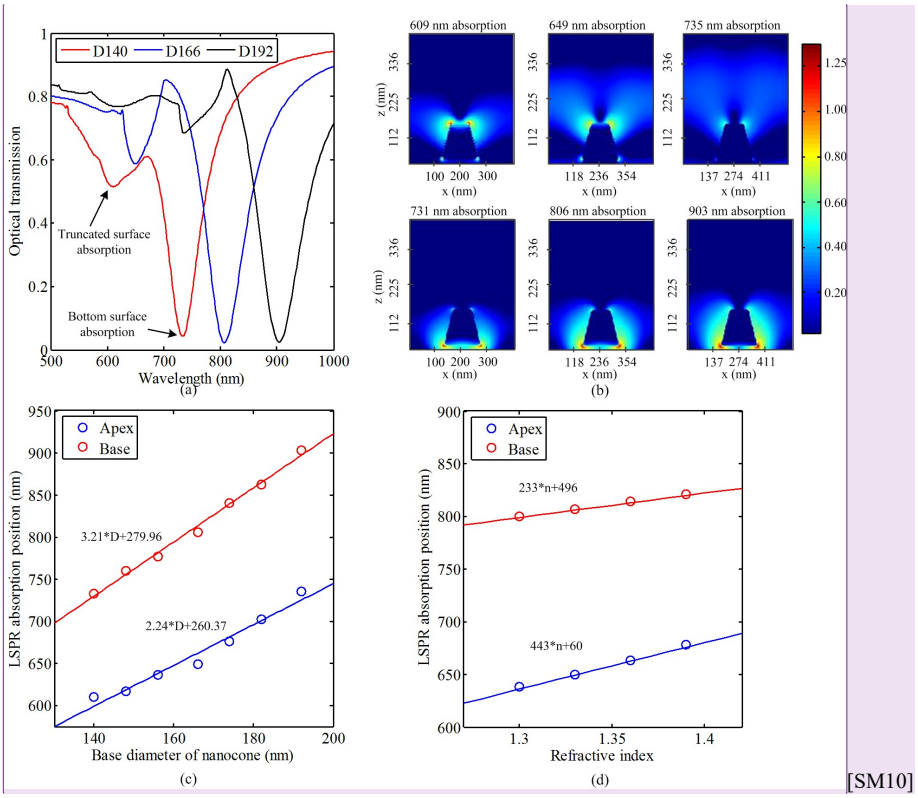


[SM10]

Figure 2. Simulated optical transmission spectra of a 150-nm-thick gold nanocones with base diameters of 140 nm, 166 nm, and 192 nm. Each nanocone had an apex diameter half of the base diameter. The nanocones were situated on a Pyrex substrate with n = 1.474 at λ = 587 nm and were contained in water with n = 1.330 at λ = 587 nm. b) Electric field distributions of nanocones with base diameters of 140 nm, 166 nm, and 192 nm (right, middle, and left images respectively at absorption wavelengths of 609 nm, 649 nm, and 735 nm (apex; top panel) and 731 nm, 806 nm, and 903 nm (base; bottom panel). c) spectral position of LSPR absorption peak from apex and base versus base diameter of the nanocone. d) Spectral position of LSPR absorption peak from apex and base of a nanocone with a 166-nm-base diameter and 150-nm-thick gold versus refractive index of the surrounding medium.

Figure 3 (a) displays simulated optical transmission data of NHA-NCAs with periodicities of 400 nm, 475 nm and 550 nm. The 3D nanostructures had resonance peaks related to SP excitation modes and LSPR interactions between the nanohole and nanocone. Figure 3 (b) shows the electric field distribution for each resonance within one pair of nanohole-nanocone of the 3D nanostructure. The 3D nanostructure with 400-nm periodicity had one resonance related to the (-1, 0) SP excitation[SM11]. Based on the electric field distribution in Figure 3 (b), the 3D nanostructure with 400-nm periodicity had LSPR coupling between the hole and apex of the nanocone at the (-1,0) resonance wavelength. The 3D nanostructures with 475-nm and 550-nm periodicities had two resonances related to the (-1, 0) and (1, 1) SPR excitations. In addition, a high electric field intensity between the nanohole and nanodisk at both the (-1, 0) and the (1, 1) resonance was observed and was due to LSPR coupling between the nanohole and the nanocone. However, the (-1, 0) resonance for the 3D nanostructure was divided into two resonances and one standalone LSPR, which resulted from an LSPR interaction between the nanohole and the nanocone (see the strong electric field intensity map on in Figure 3 (b)). The optical transmission spectra of NHA-NCA structures were experimentally observed (Figure 3 (c)). Both, simulation and experimental results, were in good agreement with respect to the (-1, 0), (1, 1), and LSPRs. However, the (0, ±1) resonances were observed for the 3D nanostructure with 475-nm periodicity in the experiment, but not in the simulation. This discrepancy could have resulted from the ±6 degree uncertainty in the illumination angle in the experiment (relative to normal incidence), which was expected to excite the (0,±1) resonance. [SM12]Figure 3 (d) displays the SPR peak positions of the 3D nanostructure with 475-nm periodicity versus refractive index of surrounding medium. The slope of the line of best fit of the resonance position versus refractive index was used to estimate the bulk SPR sensitivity of each resonance. The bulk sensitivities for the (-1, 0), the (1, 1), and the (0, ±1) resonances were 440 nm/RIU, 280 nm/RIU, and 460 nm/RIU, respectively. For the 3D nanostructure with 475-nm periodicity, the measured (-1, 0) and (1, 1)

resonance peak widths (FWHM) were 40 nm and 56 nm, respectively. Also, the FOM for the (-1, 0) and the (1, 1) resonances were 11 $RIU^{-1}$ and 5 $RIU^{-1}$, respectively. The bulk sensitivity related to the (-1, 0) of the 3D nanostructure with 550-nm periodicity was about 598 nm/RIU but the peak width of the resonance was larger than the 3D nanostructures with smaller periodicities due to the separate LSPR next to the (-1, 0) resonance.

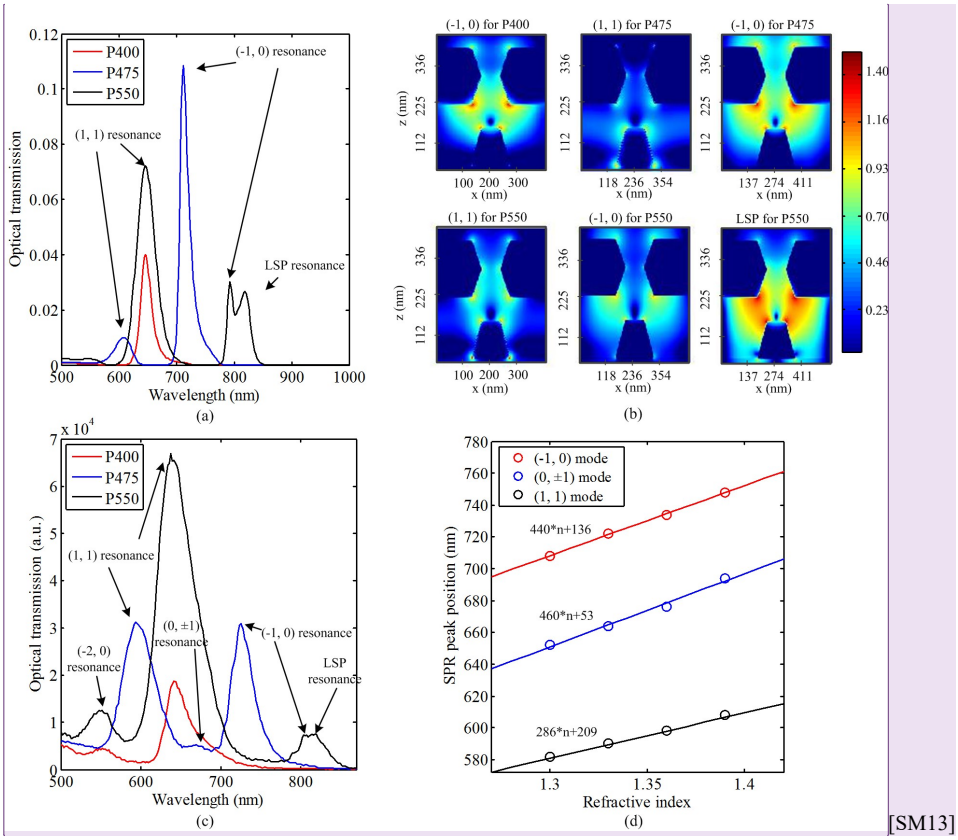


Figure 3. a) Simulated optical transmission spectra of NHA-NCA structures with 400-nm, 475-nm, and 550-nm periodicities. b) Electric field distributions of NHA-NCAs with 400-nm, 475-nm, and 550-nm periodicities at various resonance wavelengths. c) Experimentally observed optical transmission spectra of NHA-NCA structures with 400-nm, 475-nm, and 550-nm periodicities. d) Measured SPR position of the NHA-NCA structure with 475-nm periodicity as a function of refractive index of the surrounding medium.

The (-1, 0) resonance peak shift of 3D nanostructure with 475-nm periodicity in response to 20-nM, 200-nM, 2000-nM, and 3500-nM streptavidin was measured and shown in Figure 4. To find a precise (-1, 0) resonance position from each spectrum, we assessed the spectral resonance peak position using Gaussian curve fitting. The mean value among triplicate measurements ±1 standard deviation (SD) was reported in Figure 4. Moreover, the detection certainty for the 3D nanostructure was estimated based on the mean value from triplicate PBS measurements (blue solid line in Figure 4) ±2 times the average noise (blue dashed lines in Figure 4). The lowest concentration of streptavidin detectable by the 3D nanostructure with sufficient detection certainty was considered the limit of detection (LOD). The (-1, 0) resonance peak was shifted to longer wavelengths as the concentration of streptavidin increased. It was seen that the LOD for the (-1, 0) resonance of the 3D nanostructure with 475-nm periodicity was approximately 20 nM. The largest spectral resonance shift was from 200 nM to 2000 nM.

Previous work has demonstrated that a conventional NHA with 650-nm periodicity and 400-$\mu m^2$ area was capable of sensing 20 µM streptavidin by monitoring the spectral shift in the resonance [20]. The mean resonance peak shift for 20 µM streptavidin was between 3.5 nm and 4 nm. In another study, 25-nM streptavidin was detectable using a multiplexed arrangement of NHAs and a stable laser light source and a cooled CCD camera. The multiplexed method was based on differentiating signals from a NHA exposed to PBS and a NHA exposed to streptavidin. This technique improved the signal to noise ratio and thereby the LOD to 25 nM [21]. Without the use of a laser or a cooled CCD camera, our 3D nanostructure was capable of detecting 20-nM streptavidin. Also, the previous results suggested that higher LOD can be

achieved by designing a 3D nanostructure with larger periodicity (i.e. higher bulk sensitivity) [22]. Furthermore, it can be anticipated that the LOD of streptavidin with the 3D nanostructure could be further improved by implementing a stable light source and a cooled detector.

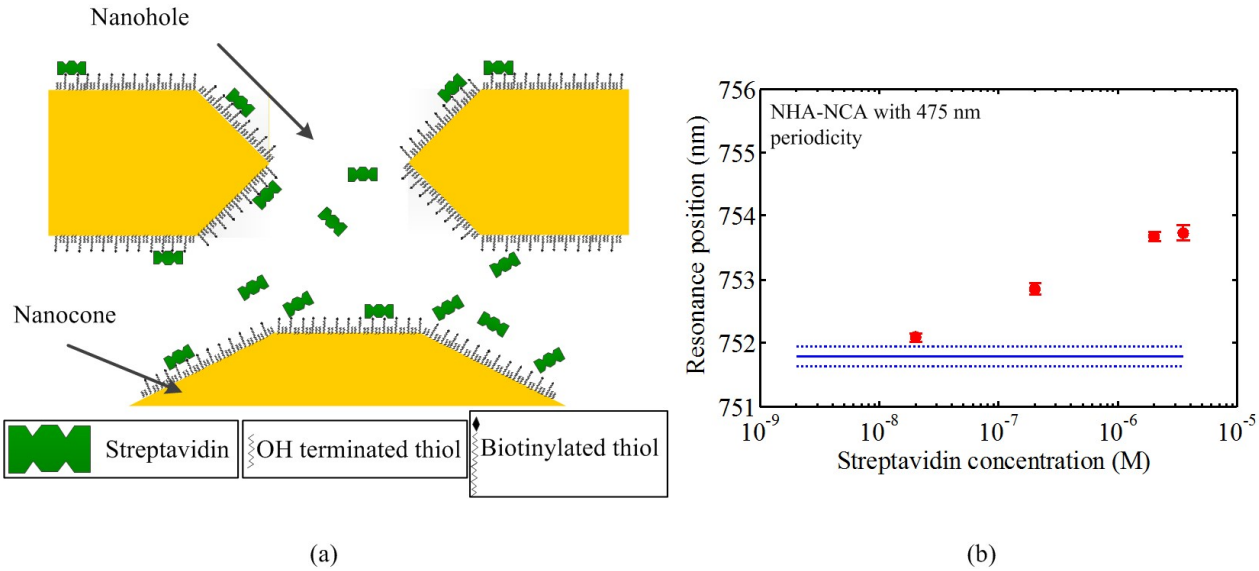


Figure 4. a) A schematic of functionalized NHA-NCA surfaces with biotinylated thiol and OH terminated thiol. Streptavidin molecules bind to biotinylated thiol. b) Symbols ± error bars represent the mean ±1 standard deviation computed from three measurements. The solid blue line represents the base line from PBS measurements (mean value among triplicate PBS measurements) and the dashed blue lines represents ±2 times the standard deviation of the PBS measurements representative of the detection threshold.

The NHA-NCA had higher bulk sensitivity and higher LOD in bio-sensing compared to a conventional NHA. Improved bulk and bio-sensitivities are probably due to a combination of factors. First, the 3D nanostructure consists of a cavity, which results in dynamic surface plasmon matching between the top and bottom surfaces of the gold NHA membrane [9]. Second, the bottom surface of the NHA membrane had an ultra-smooth gold surface as a consequence of the polished surface of the Pyrex substrate (with roughness parameter, Ra <15Å), prior to etching. Third, the simulations reveal the existence of a highly localized electric field between the nanohole and the nanocone, which explains the high sensitivity of this region of the device to changes in refractive index of the intermediate dielectric materials. One of the deficiencies of the NHA-NCA is the lower resonance transmission efficiency at the resonances than that of a conventional NHA. This was expected due to the optical absorption properties of the nanocone and nanocone shadowing effects on each incident nanohole [17].

## 4. CONCLUSIONS

A 3D metallic nanostructure consisting of a metallic film with a NHA, a cavity beneath the NHA, and a NCA at the bottom of the cavity was studied. The optical transmission resonances of the device resulted from both LSPR and SPP interactions. Several 3D metallic nanostructures were fabricated and tested by a means of simulation and experiment with respect to resonance position, bulk-SPR sensitivity, and FOM. The bulk-SPR sensitivity and FOM for the 3D nanostructures with 475-nm periodicity were found to be 440 nm/RIU and 11 $RIU^{-1}$, respectively. The structure had almost 3-fold higher FOM compared to a conventional NHA. Finally, a 3D metallic nanostructure with 475-nm periodicity functionalized with biotinylated thiol was observed capable of detecting 20-nM streptavidin. In future work, a multiplexed detection method could be used to further improve the LOD of the 3D nanostructure in bio-sensing.

## 5. ACKNOWLEDGEMENT

The authors thank Dr. Todd Simpson for his technical support at the Western Nanofabrication Facility at the University of Western Ontario (UWO). This project was funded by grants from the Natural Sciences and Engineering Research Council of Canada (NSERC) to Dr. Bozena Kaminska and Dr. Jeffrey J. L. Carson. Dr. Mohamadreza Najiminaini was supported by the MITACS program. Dr. Silvia Mittler would like to thank the NSERC BiopSys Strategic Network for financial contributions.

## REFERENCES

1. J. N. Anker, W. P. Hall, O. Lyandres, N. C. Shah, J. Zhao, and R. P. Van Duyne, "Biosensing with plasmonic nanosensors," Nat Mater **7,** 442-453 (2008).
2. H. Jiang, T. Li, E. Ertorer, J. Yang, J. Sabarinathan, and S. Mittler, "A biosensor based on periodic arrays of gold nanodisks under normal transmission," Sensors and Actuators A: Physical **189,** 474 (2013).
3. C. Valsecchi and A. G. Brolo, "Periodic Metallic Nanostructures as Plasmonic Chemical Sensors," Langmuir **29,** 5638-5649 (2013).
4. A. A. Yanik, M. Huang, A. Artar, T. Chang, and H. Altug, "Integrated nanoplasmonic-nanofluidic biosensors with targeted delivery of analytes," Appl. Phys. Lett. **96,** 021101-3 (2010).
5. T. W. Ebbesen, H. J. Lezec, H. F. Ghaemi, T. Thio, and P. A. Wolff, "Extraordinary optical transmission through sub-wavelength hole arrays," Nature **391,** 667-669 (1998).
6. A. Krishnan, T. Thio, T. J. Kim, H. J. Lezec, T. W. Ebbesen, P. A. Wolff, J. Pendry, L. Martin-Moreno, and F. J. Garcia-Vidal, "Evanescently coupled resonance in surface plasmon enhanced transmission," Opt. Commun. **200,** 1-7 (2001).
7. G. A. Cervantes Tellez, S. Hassan, R. N. Tait, P. Berini, and R. Gordon, "Atomically flat symmetric elliptical nanohole arrays in a gold film for ultrasensitive refractive index sensing," Lab Chip **13,** 2541-2546 (2013).
8. J. Henzie, M. H. Lee, and T. W. Odom, "Multiscale patterning of plasmonic metamaterials," Nat Nano **2,** 549-554 (2007).
9. M. Najiminaini, F. Vasefi, B. Kaminska, and J. J. L. Carson, "Effect of surface plasmon energy matching on the sensing capability of metallic nano-hole arrays," Appl. Phys. Lett. **100,** 063110-4 (2012).
10. L. Pang, G. M. Hwang, B. Slutsky, and Y. Fainman, "Spectral sensitivity of two-dimensional nanohole array surface plasmon polariton resonance sensor," Appl. Phys. Lett. **91,** 123112-3 (2007).
11. A. A. Yanik, A. E. Cetin, M. Huang, A. Artar, S. H. Mousavi, A. Khanikaev, J. H. Connor, G. Shvets, and H. Altug, "Seeing protein monolayers with naked eye through plasmonic Fano resonances," PNAS **108,** 11784 (2011).
12. L. K. S. Kumar, A. Lesuffleur, M. C. Hughes, and R. Gordon, "Double nanohole apex-enhanced transmission in metal films," Appl. Phy. B **84,** 25-28 (2006).
13. M. Najiminaini, F. Vasefi, B. Kaminska, and J. J. L. Carson, "Nano-hole array structure with improved surface plasmon energy matching characteristics," Appl. Phys. Lett. **100,** 043105 (2012).
14. F. Przybilla, A. Degiron, C. Genet, T. Ebbesen, F. de Léon-Pérez, J. Bravo-Abad, F. J. García-Vidal, and L. Martín-Moreno, "Efficiency and finite size effects in enhanced transmission through subwavelength apertures," Opt. Express **16,** 9571-9579 (2008).
15. R. Gordon and P. Marthandam, "Plasmonic Bragg reflectors for enhanced extraordinary optical transmission through nano-hole arrays in a gold film," Opt. Express **15,** 12995-13002 (2007).
16. N. C. Lindquist, A. Lesuffleur, H. Im, and S. Oh, "Sub-micron resolution surface plasmon resonance imaging enabled by nanohole arrays with surrounding Bragg mirrors for enhanced sensitivity and isolation," Lab Chip **9,** 382-387 (2009).
17. M. Najiminaini, F. Vasefi, B. Kaminska, and J. J. L. Carson, "A three-dimensional plasmonic nanostructure with extraordinary optical transmission," Plasmonics **8,** 217-224 (2012).
18. E. D. Palik, *Handbook of Optical Constants of Solids* (Academic Press, 1985).
19. W. L. Barnes, A. Dereux, and T. W. Ebbesen, "Surface plasmon subwavelength optics," Nature **424,** 824-830 (2003).
20. A. De Leebeeck, L. K. S. Kumar, V. de Lange, D. Sinton, R. Gordon, and A. G. Brolo, "On-Chip Surface-Based Detection with Nanohole Arrays," Anal. Chem. **79,** 4094-4100 (2007).

21. H. Im, A. Lesuffleur, N. C. Lindquist, and S. Oh, "Plasmonic Nanoholes in a Multichannel Microarray Format for Parallel Kinetic Assays and Differential Sensing," Anal. Chem. **81,** 2854-2859 (2009).
22. M. Najiminaini, E. Ertorer, B. Kaminska, S. Mittler, and J. J. L. Carson, "Surface plasmon resonance sensing properties of a 3D nanostructure consisting of aligned nanohole and nanocone arrays," Analyst (2014).